Chemical Science

Accepted Manuscript

Volume 7 | Number 1 | January 2016 | Pages 1–812

Chemical Science

www.rsc.org/chemicalscience

ISSN 2041-6539

ROYAL SOCIETY OF CHEMISTRY

EDGE ARTICLE
Francesco Ricci et al.
Electronic control of DNA-based nanoswitches and nanodevices

175 YEARS

This is an Accepted Manuscript, which has been through the Royal Society of Chemistry peer review process and has been accepted for publication.

Accepted Manuscripts are published online shortly after acceptance, before technical editing, formatting and proof reading. Using this free service, authors can make their results available to the community, in citable form, before we publish the edited article. We will replace this Accepted Manuscript with the edited and formatted Advance Article as soon as it is available.

You can find more information about Accepted Manuscripts in the author guidelines.

ROYAL SOCIETY OF CHEMISTRY

rsc.li/chemical-science

Journal Name

ARTICLE

Highly Enantioselective "Inherently Chiral" Electroactive Materials Based on the 2,2'-Biindole Atropisomeric Scaffold

Serena Arnaboldi,[a] Tiziana Benincori,*[b] Andrea Penoni,[b] Luca Vaghi,[c] Roberto Cirilli,[d] Sergio Abbate,[e] Giovanna Longhi,[e] Giuseppe Mazzeo,[e] Sara Grecchi,[a] Monica Panigati[a,f] and Patrizia Romana Mussini*[a]

Chiral oligothiophene monomers with C_2 symmetry, based on 3,3'-bithiophene atropisomeric cores with high racemization barriers, have been recently shown to provide excellent chiral starting materials with high electroactivity for the easy preparation of enantiopure electroactive films endowed with powerful chirality manifestations. We now introduce an inherently chiral monomer based on a 2,2'-biindole core, as the prototype of a new inherently chiral monomer family, whose properties could be modulable through functionalization of the pyrrolic N atoms. By fast, regular electrooligomerization the new monomer yields inherently chiral films with high, reversible electroactivity and, above all, impressive enantioselectivity towards very different chiral probes, some of pharmaceutical interest, as general-scope electrode surfaces. Such results, while opening the way to a new, attractive inherently chiral selector class, nicely confirm the general validity of the inherent chirality strategy for chiral electrochemistry. Furthermore, the enantioselectivity of the new selectors not only holds with electroactive chiral probes, but also with circularly polarized light components as well as electron spins, resulting in good chiroptical and spin filter performances, which suggests fascinating correlations between the three contexts.

Introduction

Thiophene-based monomers with C_2 symmetry, including either an atropisomeric 3,3'-bibenzothiophene (**BT$_2$-T$_4$**)[1] or a 3,3'-bithiophene core[2] with high racemization barriers, have been recently shown to provide excellent chiral starting materials of high electroactivity for the easy chemical or electrochemical preparation of enantiopure electroactive films, endowed with powerful chirality manifestations. As chiral electrode surfaces they show outstanding enantioselectivity toward the enantiomers of different chiral probes, resulting in very different peak potentials, so that they can be recognized without preliminary separation steps;[1,2,4-6] thus, they could provide outstanding tools for chiral voltammetry (and in perspective, more generally, chiral electrochemistry), particularly considering that most of the many previous approaches to this target suffered from one or more

drawbacks, resulting *e.g.* in current rather than in potential differences for the probe enantiomers, being specifically tailored for a single probe, being of difficult and/or expensive preparation, lacking robustness, and so on.[7,8] At the same time, the same films exhibited chiroptical properties (circularly polarized luminescence as well as intense circular dichroism, reversibly controlled by electrochemical polarization)[1,3,4] and, very recently, unprecedented molecular spin filter performances.[9] The search of efficient molecular spin filters as an attractive alternative for inorganic active materials in spintronics is a hot topic, prompted by the inspiring works of Ron Naaman and collaborators describing "Chiral Induced Spin Selectivity" (CISS) effects of chiral molecular materials. They report *e.g.* significant spin polarization in photo-ejected electrons transmitted through an enantiopure thin layer on Au as well as small but significant current differences for achiral redox probes in magnetoelectrochemistry experiments on ferromagnetic electrodes functionalized with enantiopure chiral molecular layers, inverting magnetic field orientation.[10-13] The authors explain such effects in terms of different transmission probabilities of α and β electrons through the chiral layers. In this context, the above mentioned spin filter experiments by some of us appear groudbreaking since potential differences are observed rather than current ones, working with chiral oligothiophene-based oligomer films on ITO electrodes under an applied magnetic field.[9] Spin-modulated electrochemical potentials indeed appear an attractive tool, giving the convenience of electrode potential for selection, activation, or transduction purposes.

The outstanding enantiodiscrimination performances of our electroactive films based on atropisomeric elements were justified by their peculiar design, implying (*i*) "inherent chirality", since the stereogenic element coincides with the functional

[a.] *Dipartimento di Chimica, Università degli Studi di Milano, Via Golgi, 19, 20133 Milano (Italy) E-mail: patrizia.mussini@unimi.it*

[b.] *Dipartimento di Scienza e Alta Tecnologia, Università degli Studi dell'Insubria, via Valleggio 11, 22100 Como (Italy) E-mail: tiziana.benincori@uninsubria.it*

[c.] *Dipartimento di Scienze dei Materiali, Università di Milano-Bicocca, via R. Cozzi 55, 20125 Milano (Italy)*

[d.] *Istituto Superiore di Sanità, Centro nazionale per il controllo e la valutazione dei farmaci, Viale Regina Elena 299, 00161 Roma (Italy)*

[e.] *Dipartimento di Medicina Molecolare e Traslazionale, Università degli Studi di Brescia, Viale Europa 11, 25123 Brescia (Italy)*

[f.] *Istituto per lo Studio delle Macromolecole, Consiglio Nazionale delle Ricerche (ISMAC-CNR), Via E. Bassini, 15, 20133 Milano (Italy)*
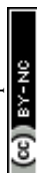
group determining the specific material property (here, electroactivity), *i.e.* the whole main conjugated backbone featuring a tailored torsion with a racemization barrier too high to be overcome in the working conditions, so that the monomer exists as two very stable enantiomers;[2] (*ii*) high regioregularity, since the monomers have equivalent, homotopic terminal positions for oligomerization, so that the monomer torsion cannot but propagate into regio- and stereoregular foldamer structures (of course retaining the same configuration of the starting monomer). Such very stable foldamers can warrant powerful and robust chirality manifestations, much higher than chiral polymers from achiral monomers grown in asymmetric conditions, and even than chiral polymers, in which the stereogenic element consists in stereocentres external to the main conjugated backbone.[8] An additional important feature is that, in the case of the 3,3'-bibenzothiophene-based inherently chiral monomer, the oligomer mixture obtained by (electro)-oligomerization was found to include many cyclic terms,[4,14] that can be regarded as a mixture of attractive chiral cavities of different dimensions and with many available heteroatoms, promoting diastereomeric interactions with chiral guests.

To confirm the general validity of the above strategy and related interpretation, as well as to explore the possibility to modulate functional properties, it is particularly important to explore materials derived from inherently chiral starting monomers of different chemical nature. Song and coauthors recently studied a series of monomers with thiophene-based wings and binol atropisomeric cores,[15] preparing electrode surface films and testing them with aminic probes giving acid/ base interactions with the core hydroxy groups. Some enantioselectivity manifestations were observed, *e.g.* in terms of differences in potential *vs* concentration trends for the enantiomers of the chiral probe, working in potentiometric although less useful for enantiorecognition purposes than the above CV tests. Such interesting observations do not however look decisive for the above discussed electroanalytical applications.
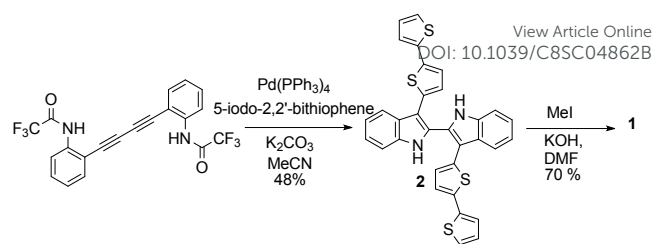
Scheme 1.

In this context, we are considering the 2,2'-biindole scaffold as a very appealing candidate as atropisomeric core of inherently chiral monomers. In fact, it is electron richer and thus more easily oxidable than the thiophene-based cores; moreover, unlike them, it can be functionalized on the nitrogen atoms, a feature that can be exploited to prepare a wide palette of monomers, with fine modulation of key properties, *e.g.* solubility, important for chemical processing, as well as torsional angle.

In this work we introduce the 3,3'-bis(2,2'-bithiophen-5-yl)-1,1'-dimethyl-1*H*,1'*H*-2,2'-biindole (**1**), nicknamed as **(N-Me-IND)₂-T₄** (**Figure 1**), as a very convenient starting monomer to prepare inherently chiral films performing as general-scope electrode surfaces of high and reversible electroactivity and impressive enantioselectivity towards very different electroactive chiral probes, also of pharmaceutical interest; at the same time, they also exhibit high chiroptical activity as well as impressive spin filter features. This highlights fascinating correlations between the three contexts, for which we propose a tentative sketch.

Results and Discussion

2.1 The starting inherently chiral monomer as a racemate

2.1.1. Synthesis

The synthesis of racemic monomer **1**, reported in **Scheme 1** and detailedly described in **SI.1.1**, was planned according to an interesting variant of the Larock reaction[16] presented by Abbiati *et al.*[17] for the preparation of 2,2'-biindole derivatives functionalized in position 3 with different aryl substituents.

The reaction, catalyzed by Pd(0), requires a double alkyne derivative, namely the 2,2,2-trifluoro-*N*-(2-(4-[2,2,2-trifluoro-acetylamino-phenyl]-buta-1,3-diynyl)-phenyl)-acetamide and a suitable aromatic haloderivative. We exploited this strategy using the 5-iodo-2,2'-bithiophene, obtained in turn by direct iodination of 2,2'-bithiophene with *N*-iodosuccinimide in 1:1 CHCl₃:CH₃COOH solution.[18] The reaction was carried out in refluxing acetonitrile using palladium(tetrakis) as catalyst and K₂CO₃ as base. This approach allowed us to perform in a single step the formation of the interanular bond between the two indole units and their functionalization with the bithienyl units. Racemic monomer **1** was obtained in good yields by reaction of the bisanion of **2**, generated employing KOH in *N,N*-dimethylformamide at 0 °C, with methyl iodide.

2.1.2. Structural and electronic peculiarities of the inherently chiral monomer

The **(N-Me-IND)₂-T₄** monomer is a remarkable tool with attractive peculiarities, which were highlighted by a pool of complementary multitechnique studies carried out with **BT₂T₄** as a
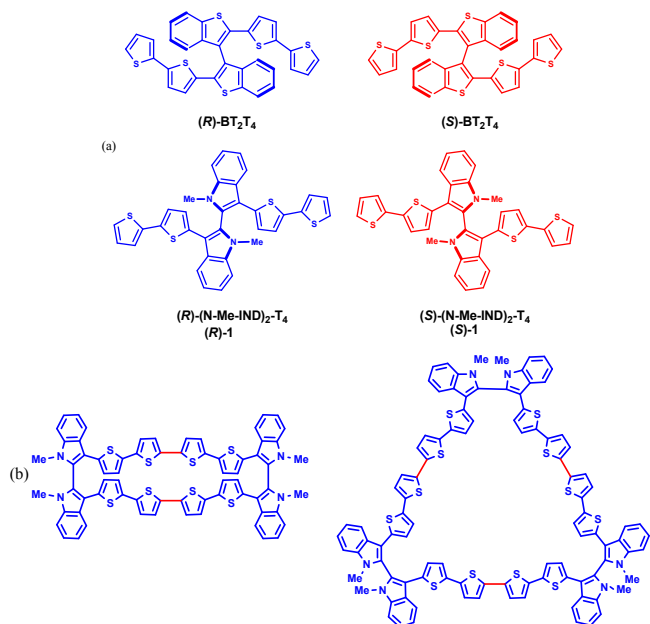

Figure 1. (a) Enantiomers of inherently chiral monomers discussed; (b) Planar molecular formulas of cyclic dimers and trimers of monomer **1** (red bonds indicate the oligomerization sites).

benchmark, which included theoretical computations (detailedly accounted for in **SI.2**), chiral HPLC off-column configuration stability studies (**SI.3**), cyclic voltammetry, CV (**Figure 2a-d, SI.4**), electronic absorption and emission spectroscopy (**Figure 2e, SI.5**)

The monomer is a C_2 symmetry atropisomeric system, consisting of two equal moieties with a torsional barrier being 27 kcal mol^{-1} according to computations (**SI.2** with related **Table SI.2.1** and **Figures SI.2.1-SI.2.4**) and 29.9 kcal mol^{-1} according to off-column racemization experiments analyzed by enantioselective HPLC (**SI.3**). Such barrier is high enough to have stable **(R)**- and **(S)-(N-Me-IND)$_2$-T$_4$** enantiomers at room temperature (**Figure SI.2.5**), while also allowing some partial residual communication between the two moieties through the central link, besides through-space interactions. Such communication is more efficient than in **BT$_2$T$_4$**, which has a significantly higher torsional barrier, 43 kcal mol^{-1}, as well as a nearly 90° torsional angle (**Figure SI.1.1**)[1].

The two moieties are quite active both electrochemically, as redox sites (**SI.3**) and spectroscopically, as chromophores (**SI.4**), the two features being strictly interconnected. HOMO and LUMO orbitals mainly involve the pyrrole-bithiophene PTT conjugated systems (**Figure SI.2.4**), and are therefore both shifted to much higher energies than in the **BT$_2$T$_4$** case (which involves terthiophene TTT conjugated systems) consistently with the electron-richer nature of the pyrrole ring respect to the thiophene one. This is evident by the significant negative potential shifts of the corresponding CV features (easier oxidation, more difficult reduction **Figure 2**, **Table 1**). Consistently, the HOMO-LUMO gaps are similar to the **BT$_2$T$_4$** ones[19,20] (**Table 1**), but translated to higher energies.

The presence of the pyrrole ring also results in an asymmetry in the main conjugated system with respect to the **BT$_2$T$_4$** case, with significant localization of the HOMO on the pyrrole side (*i.e.* on the monomer core) and of the LUMO on the bithiophene side (*i.e.* on the monomer terminals). This is confirmed by electronic spectroscopy (**SI.5**), in which absorption and emission wavelengths exhibit some solvatochromism, pointing to a charge transfer character of the electronic transition (**Figure 2e**), and above all by CV experiments, where, unlike the **BT$_2$T$_4$** case, first oxidation

appears chemically reversible and with no coupling follow-up (**Figure 2a**); this is consistent with stable radical cation formation close to the molecule core. Instead to achieve oligomerization it is necessary to activate the thiophene wings by potential cycling around the relevant, much more positive, oxidation peak. (**Figure 2c**; see also Figure **SI.2.3** for characterization of charged species via DFT calculations).

Interestingly, the presence of two equivalent, partially interacting PTT moieties/redox sites nicely results in a twin-peak system for the monomer first oxidation in CV, corresponding to the formation of two partially interacting radical cations, each one on a PTT moiety, each of them mostly localized on the pyrrole ring (as above discussed). In other words, partial reciprocal interaction results in loss of degeneracy between the two equivalent redox sites, which are therefore activated at different potentials/energies. Such peak splitting is dependent on solvent polarity; in particular, the higher charge screening ability of acetonitrile respect to dichloromethane results in twin peak merging; concurrently chemical reversibility appears to decrease, too, at least at low scan rates (**SI.4**).

One could dare a parallelism between the loss of degeneracy of the two PTT moieties as redox sites and the loss of degeneracy as chromophores in absorption spectroscopy, in terms of "exciton coupling" due to interaction between electric dipole transition moments, resulting in a splitting in absorption wavelengths for the two moieties/chromophores. This Davydov splitting[21,22] is evidenced in electronic circular dichroism ECD spectroscopy (discussed further on in paragraph **5.1.a**) by a symmetrical couplet for the monomer enantiomers (**Figure 3**) centered close to the UV-vis absorption maximum wavelength (**Figure 2e**). Interaction of neighbour electric fields in space can justify both phenomena. This analogy, or more appropriately, connection, between redox potential splitting and wavelength splitting in atropisomeric conjugated systems is to our knowledge here pointed out for the first time. Careful reexamination of former works[19,20] confirms the simultaneous presence of spectroscopic (Davydov) splitting and CV peak splitting in other atropisomeric inherently chiral systems with two equivalent redox sites/chromophore moieties, as discussed in more detail in **SI.6**)

Table 1. Electrochemical and photophysical properties of monomer **1** compared to **BT$_2$-T$_4$**.[19,20] Photochemical characterizations were carried out in air-equilibrated dilute solutions at room temperature.

	$E_{p,c}$ vs Fc$^+$|Fc/ V	$E_{p,a}$ vs Fc$^+$|Fc/ V	$E_{LUMO, EC}$[a] / eV	$E_{HOMO, EC}$[a] / eV	λ_{abs}/ nm ($10^4\varepsilon$ / M^{-1}cm^{-1})	λ_{em}/ nm (Φ)	τ / ns	H−L gap / eV
(N-Me-IND)$_2$-T$_4$								
ACN	-2.62, -2.71	**0.47**;0.82; 0.99	-2.18	-5.27	364 (3.13)	503 (0.15)	1.1	3.09[b] (3.41)[c]
DCM	n.d.	**0.38,0.56**;0.78;0.87		-5.18	367	500 (0.16)		(3.38)[c]
Toluene					358	523 (0.08)		(3.47)[c]
BT$_2$-T$_4$								
ACN[19]	-2.28	0.78	-2.52	-5.58	372 (4.80)	507 (0.16)	1.7	3.06[b] (3.33)[c]
DCM [20]	n.d.	0.67,0.80		-5.47	378	505 (0.18)		(3.28)[c]
Toluene					371	507 (0.15)		(3.34)[c]

[a] Estimated as $E_{LUMO(HOMO), EC}$ = -1e ($E_{p,Ic(Ia)}$/ V vs Fc$^+$\|Fc + 4.8/ V Fc$^+$\|Fc vs 0); [b] Electronic gap; [c] Optical bandgap

Chemical Science Accepted Manuscript

3. Conversion of the monomer into oligomer films

The monomer features can be propagated and amplified due to regioregularity, converting the monomer into an oligomer film, which can be done either chemically or electrochemically. Chemical oxidation of racemic **1** can be performed with an excess of $FeCl_3$ in $CHCl_3$ at room temperature, as previously described for **BT₂-T₄**, and processed as accounted for in the Experimental section. High Resolution Laser Desorption Ionization (HR-LDI) experiments reveal that the oligomer mixture contains dimers and trimers (height peak ratio 40), their isotopic patterns unequivocally demonstrating that all of them are fully conjugated macrocycles (**Figure SI.7.1**). Concurrently, HPLC analysis on Chiral Stationary Phase (CSP) (CD detector) of a pure sample of cyclic dimers, isolated by column chromatography, demonstrates the presence of enantiomers and meso-compound in quite similar amounts (**Figure SI.7.2**).

Oligomer films can also be directly electrodeposited on a suitable electrode support by repeated potential cycling around the potential corresponding to the third oxidation peak (the first one involving the bithiophene wings with free terminals); fast formation of an electroactive film on the electrode surface is observed in DCM (**Figure 2c**); the growth is even faster upon further widening the oxidative cycle.
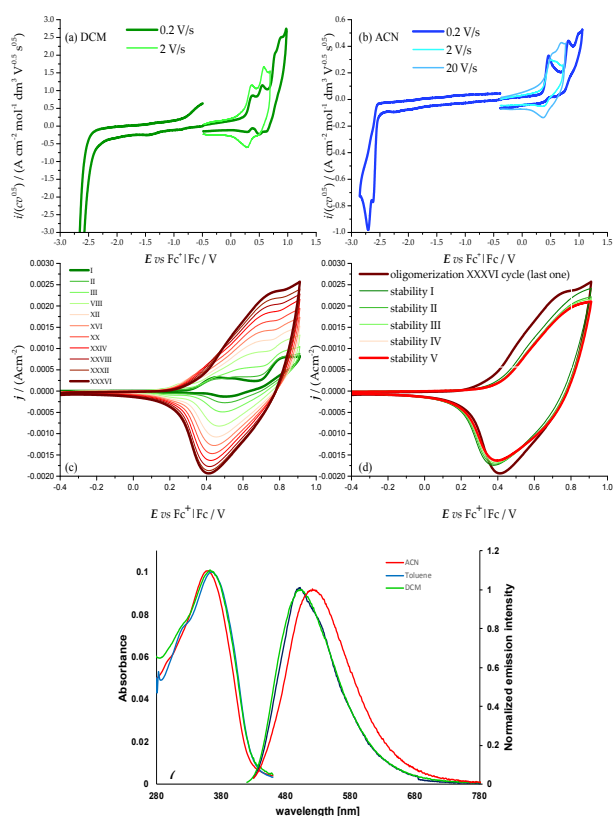
The films show good stability upon subsequent potential cycling in monomer-free solution, as required for use as enantioselective electrode surface (**Figure 2d**). The onset potential for the film is only slightly more negative than the starting monomer one, consistently with the oxidation potentials of the bisindole core and of linear tetrathiophene units (which are formed upon monomer coupling).

4. Preparation of enantiopure monomer and oligomer selectors

The antipodes of the monomer **1** can be successfully separated on a semi-preparative scale by HPLC on the polysaccharide-based Chirapak IB CSP under chlorinated normal phase conditions. **Figure 3** shows the analytical HPLC chromatogram of 1 obtained by on-line CD detection and the check of the enantiomeric purity of the isolated antipodes. The $[\alpha]_{20}^D$ values are +808° and -818° (0.1 M in $CHCl_3$) for the first and the second eluted enantiomer, respectively.

From each enantiopure monomer antipode the corresponding enantiopure oligomer film can then be easily obtained. In fact both enantiomers undergo very fast and regular electrooligomerization in DCM + TBAP 0.1 M on GC as working electrode at 0.2 V s⁻¹ potential scan rate, cycling 36 times around the fourth oxidation peak (**Figure SI.8**).

5. Enantiodiscrimination performances by enantiopure selectors

5.1 Interaction with circularly polarized light L- and D-components

5.1.a Enantiopure monomers

The monomer antipodes show, as expected, enantioselectivity towards the left-handed L and right-handed D circularly polarized light components, with clear-cut differences in (*i*) L *vs* D absorption, resulting in intense circular dichroism[23-26] spectra, both electronic (ECD, **Figure 3b**) and vibrational (VCD, **Figure 3d**), as well as in (*ii*) L vs D emission, resulting in circularly polarized luminescence[23-26](CPL, **Figure 3c**).

ECD and VCD experimental spectra are reported in **Figure 3b** and **3d**. As already mentioned, they are characterized by a strong "exciton coupling" between the two equal chromophores corresponding to the monomer moieties, which results in loss of degeneracy in the absorption wavelength λ_{abs} ("Davydov splitting"). This splitting, unperceivable in the UV-vis absorption spectrum, is evidenced in the ECD one by the dominating couple of bands with maxima/minima at 347 and 390 nm, specular for the two enantiomers and intersecting each other on the λ axis at 364 nm,[27] close to the UV-vis absorption maximum. Also VCD spectra, while displaying few very weak features below 1300 cm⁻¹, contain a good number of (+,-) couplets above 1300 cm⁻¹, again as a consequence of the molecule C_2-symmetry.

Figure 2. CV patterns of monomer **1** in (a) DCM and (b) ACN, with 0.1 M TBAPF₆ supporting electrolyte, on GC electrode. Oxidative and reductive half cycles are considered separately to avoid electrode conditioning by electron transfer products; (c) Electrooligomerization of monomer **1** (0.00093 M in DCM + 0.1 M TBAP) on GC electrode by oxidative potential cycling at 0.2 V/s. (d) Stability cycles in monomer-free solution; (e) Solvent effect in the absorption and emission spectra of **1.**

Journal Name

ARTICLE

The exciton coupling in ECD spectra also provides a clue concerning the enantiomer absolute configuration; in particular, the couplet is positive (*i.e.* with the positive component at lower energy/longer wavelength) for the first eluted enantiomer (**I**) and negative for the second eluted one (**II**). According to the rules of Harada, Nakanishi and Berova,[27] this points to *P* and *M* helicity, respectively, corresponding to *S* and *R* axial stereogenicity for the present atropisomeric **I** and **II** monomer antipodes. A confirmation comes from the comparison of ECD experimental spectra with those calculated according to DFT and TD-DFT. As detailedly accounted for in **SI.2** with related **Table S2.1**, the number of conformers participating in shaping up the spectra is pretty large, the maximum population factor being less than 15%. All conformers are characterized by a positive value of the central δ dihedral angle, with values comprised between 115° and 80°; dihedral angles φ1 and φ2, next to δ, are either ca. ±35° or ca. ±145°, while ϑ1 and ϑ2 are either ca. ±160° (s-trans bi-thiophenes) or ca. ±30° (s-cis bi-thiophenes). Importantly, TDDFT calculations on all conformers give the positive exciton couplet observed in the ECD spectrum for the 1st eluted enantiomer, with maxima/minima at 347 and 390 nm (while the minor features between 290 and 190 nm are not as exactly reproduced).

Figure 4 reports the ECD spectrum computed as weighted average of calculated spectra of all conformers.
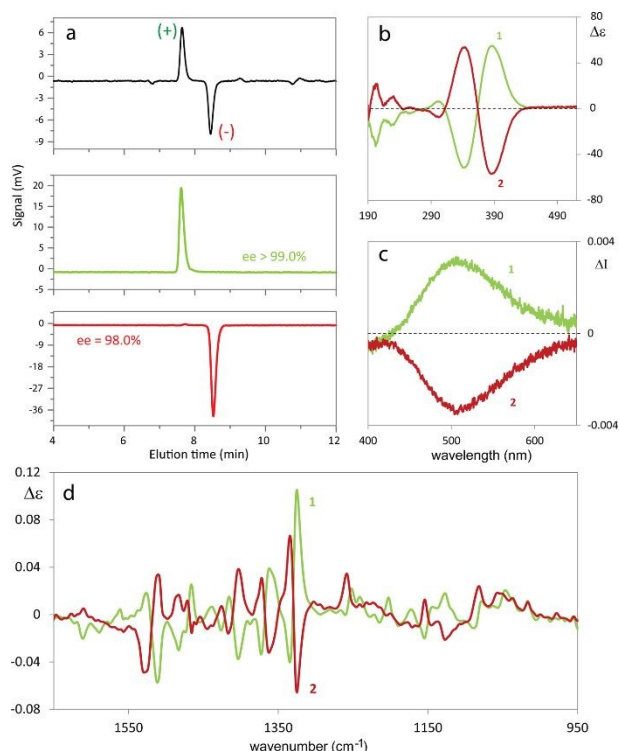

Figure 3. (a) Analytical HPLC resolution of **1** and check of the enantiomeric purity of the fractions collected on a semipreparative scale. Column: Chiralpak IB (250 mm x 4.6 mm I.D.), eluent: *n*-hexane-CH₂Cl₂ -ethanol 100:5:1, flow rate: 1 cm³ min⁻¹, temperature: 25°C, detector: CD at 380 nm; (b) Experimental Electronic Circular Dichroism (ECD) spectra of both enantiomers of **(N-Me-IND)₂-T₄**; **I** and **II** designate the elution order. (c) Experimental Circularly Polarized Luminescence (CPL) spectra (d) Vibrational Circular Dichroism (VCD).
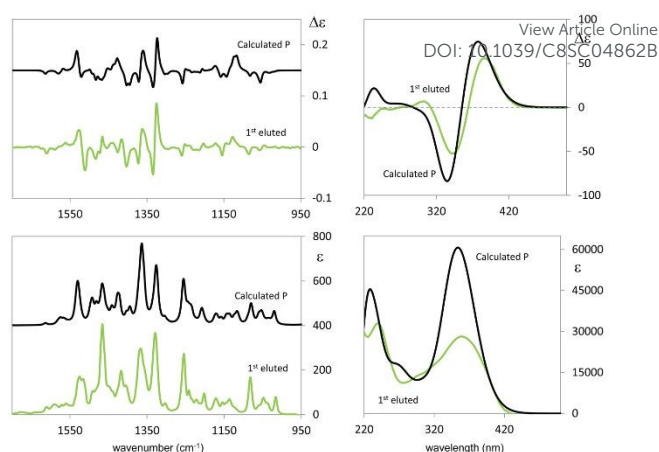
Figure 4: Comparison of experimental and calculated VCD and IR spectra (left) and comparison of experimental and calculated ECD and absorption UV spectra (right): VCD experimental data are for the semi-difference of **I** and **II** eluted enantiomers; calculated data are for the (*S*) enantiomer of **(N-Me-IND)₂-T₄**. Calculated wavenumbers in the IR range have been scaled by 0.98. Calculated wavelengths in the UV range have been shifted by 10 nm.

The calculated wavelength of the first electronic transition is similar for all conformers, in the 320-360 nm range (*i.e.* 3.45-3.87 eV), a little higher than the first observed maximum/minimum, but it should be considered that a blue shift is expected when employing CAM-B3LYP functional. By inspecting the molecular orbitals involved in the couplet (see **Figure SI.2.5**), one may see that the transitions giving rise to the two features at 390 and 347 nm are originated by transitions from HOMO and HOMO-1 orbitals localized on the pyrrole rings and the two nearby thiophene rings, to LUMO and LUMO+1 orbitals localized on the two bithiophene wings; this is consistent with the above discussion on the racemate monomer features in paragraph **2.1**.

In the case of VCD spectra, two couplets between 1320 and 1360 cm⁻¹ are clearly positive for antipode **I** and negative for **II**, and one couplet at ca. 1500 cm⁻¹ is negative for **I** and positive for **II**.[21-26] Also in this case spectra have been calculated for each conformer (**Figure SI.2.6**), and, again, the weighted averages of IR and VCD calculated spectra are in good correspondence with the experimental ones (**Figure 4**).

Not only absolute configuration is unambiguously assigned, but sensitivity to conformational structure can be recognized.

The features corresponding to the VCD couplets at 1320 and 1360 cm⁻¹ can be associated to vibrational exciton coupling[28-33] mainly involving indolic in-plane bendings (see **Figure SI.2.7**); in particular, the first one is common to all conformers while the second one is sharper for conformer 1t (φ1 and φ2 values of about ±150°). Instead the doublets at 1250 cm⁻¹ (scaled wavenumber) and at 1500 cm⁻¹ can be assigned to CH in plane bendings delocalized on thiophenes and indoles, and may be assumed as a signature of conformers with φ1 and φ2 values of about ±35°, *e.g.* conformer 2t: the observed weak intensity is due to the presence of the other conformers. Instead the negative feature at 1400 cm⁻¹ is common to all structures and can be assigned to the umbrella mode of the indole methyl groups.
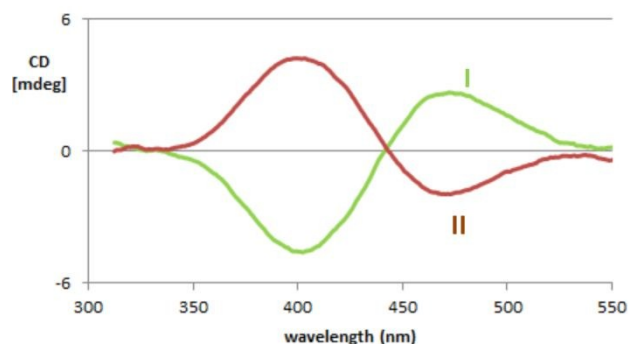
Figure 5 Experimental Electronic Circular Dichroism (ECD) spectra of both enantiomers of **(N-Me-IND)₂-T₄** films; **I** and **II** designate the elution order.

As mentioned above, the high enantiodiscrimination ability of monomer **1** antipodes also concerns polarized light emission besides absorption. Neat CPL spectra have been recorded with our home-built apparatus and are reported in **Figure 3**.[34] The single CPL band is positive for the first eluted enantiomer **I** and bears the same sign as the longest wavelength feature of the ECD couplet, as expected when the first excited state has similar geometrical and electronic structure as the ground state.[35-37] The value for the luminescence dissimmetry factor g_{lum}= $2(I_L-I_R)/(I_L+I_R)$ (with I_L and I_R denoting the intensities of the left-hand and right-hand circularly polarized emitted light components) is about 0.3×10^{-2}, which can be considered quite large for non-metal complex organic compounds in solution.[24-26] Actually the situation met in the present case, as well as for the previously studied **BT₂-T₄**,[4] monomer, looks more like the one met for the thia-bridged triarylamine heterohelicenes,[38] defined "helical-responsive", rather than simpler helicene cases,[37] where it was defined "substituent-sensitive". In fact, large ECD features correspond to large CPL features and bear the same sign, irrespective of small perturbation from substituents.

Such intense CPL makes **(N-Me-IND)₂-T₄** an attractive candidate as a material for optoelectronic devices.

5.1.b Enantiopure films

Electrodeposited films have been characterized by ECD spectroscopy, too. A couplet is observed again, but at higher wavelengths, as expected, due to the increase in conjugation upon oligomerization. The couplet is not completely symmetric, as observed also in the case of **BT₂-T₄**,[3] as a result of contributions from dimers (cyclic or non-cyclic) and trimers. Besides, the intensities of the two ECD components of the exciton couplet are different, unlike for the monomer. This may be related to the presence of oligomers of different size and shape, even though other explanations cannot be excluded.

5.2 Interaction with *R*- and *S*- antipodes of chiral molecular probes

The enantiodiscrimination ability of enantiopure oligo-**1** films is also outstanding when they are applied as inherently chiral electrode surfaces for the electroanalytical discrimination of enantiopure redox active probes with no preliminary separation step.

Very successful CV tests were carried out with three chiral electroactive molecular probes with different bulkiness, chemical nature and electrochemical activity (**Figure 6**). Model chiral probe *N,N*-dimethy-1-ferrocenylethylamine can be regarded as a benchmark given that it displays an electrochemically and chemically reversible oxidation process in a region where the film is uncharged (**Figure 6a**), being the half-wave potential 0.35 V *vs* SCE on bare GC electrode. Enantioselectivity tests, performed in DCM + TBAP 0.1 M, revealed a spectacular CV peak potential separation of 270 mV between the (*S*)- and (*R*)-antipode of *N,N*-dimethyl-1-ferrocenylethylamine, evaluated as average of three independent repetitions. This outstanding separation is the highest observed so far in our performed tests with this model probe on inherently chiral thiophene-based films. [1,2,4-6]

We have also verified that the probe/surface interactions underlying the enantiodiscrimination process are reversible and non-destructive towards the chiral film, probably as a consequence of the full chemical reversibility of the probe electron transfer. In fact, the probe-free film can be easily recovered by performing a few CV cycles around the first oxidation potential in a blank solution. This enabled to perform multiple subsequent enantiorecognition tests, alternating the (*S*) and (*R*) probe, on both the enantiomorphic surfaces, starting from either enantiomer.The second chosen analyte was (*S*)-(+)-ketoprofen, a nonsteroidal anti-inflammatory drug with analgesic and antipyretic effects. Enantiorecognition tests were performed, as in the previous experiments, in dichloromethane with TBAP as supporting electrolyte. This second case study is very interesting, because it provides an example of enantiodiscrimination based on a reduction process, respect to the formerly reported oxidation cases. In particular a large, reproducible peak potential difference (about 330 mV) is observed for the carbonyl reduction in the benzophenone system adjacent to the stereogenic center, working on either enantiomer of the indole-based film (**Figure 6b**). It should be noted that in this case, since only one antipode of the pharmaceutical probe was available, the discrimination was verified only by inverting the configuration of the inherently chiral selector (*i.e.* the film). The last tested molecule is L-3,4-dihydroxyphenylalanine (L-DOPA), active substance for the control of akinesia commonly used in the treatment of Parkinson's disease, in a real matrix, *i.e.* as the main component of the Madopar® drug in combination with benserazide. The latter acts as L-DOPA decarboxylation inhibitor, avoiding its bioconvertion into inactive dopamine by the peripheral decarboxylases before reaching the brain. The weight ratio of L-DOPA and benserazide in Madopar® is 4:1 (even higher, 84%, if we consider the mole percentage). Again the enantiopure inherently chiral surface was prepared by monomer electrooligomerization in DCM, but in this case
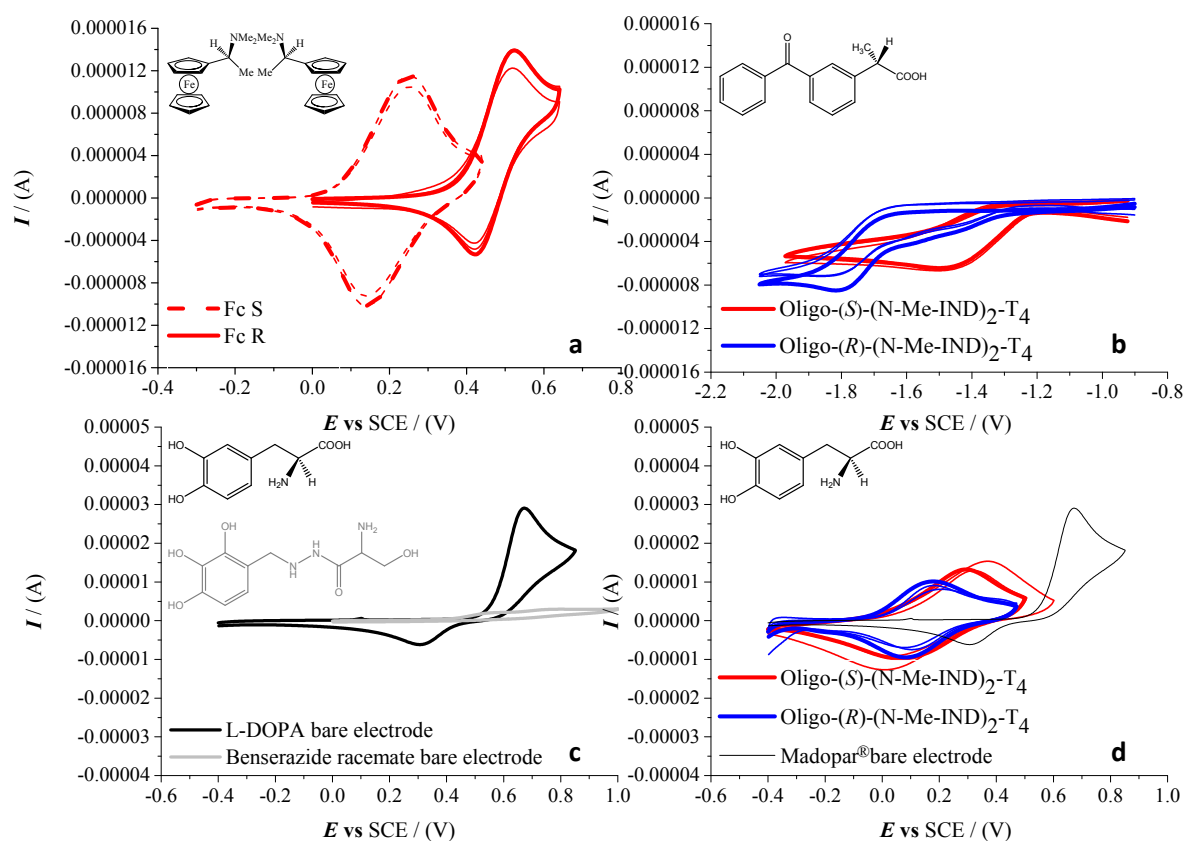
Figure 6. (a) Enantioselection on the enantiopure film oligo-**(S)-(N-Me-IND)₂T₄** towards (S)- and (R)-N,N-dimethyl-1-ferrocenylethylamine (Fc S and Fc R, dashed and solid lines, respectively). (b) Enantioselection on enantiopure films oligo-**(S)-(N-Me-IND)₂T₄** and oligo-**(R)-(N-Me-IND)₂T₄** (red and blue lines, respectively) towards (S)-(+)-ketoprofen. (c) CVs of L-DOPA (black line) and beserazide (grey line) with a 1:4 weight ratio, recorded on bare GC electrode. (d) Enantioselection on enantiopure films oligo-**(S)-(N-Me-IND)₂T₄** (red) and oligo-**(R)-(N-Me-IND)₂T₄** (blue), towards (L)-DOPA 1.9 mg (in tablet) together with Madopar® signal (black) on bare GC electrode. In (a), (b) and (d) experiments, repetition tests have been performed for each probe + selector combination.

enantiodiscrimination tests were carried out in an aqueous HCl solution at pH 2, due to the insolubility of the analyte in the organic medium. The CV pattern of the Madopar® on bare electrode (line black, **Figure 6d**), with a single oxidation peak at 0.67 V (SCE), is comparable as form and consistent in position (considering the pH effect) with that of pure L-DOPA (reported in a previous work at 0.35 V (SCE) in a pH 7 buffer solution and at 0.53 V (SCE) in a pH 4 one [5,6]). Preliminary tests were carried out recording signals of L-DOPA and benserazide separately but using the same 1:4 weight ratio of the formulation of Madopar®; in such conditions the benserazide signals, as shown in **Figure 6c**, are practically overlapped by the much higher L-DOPA peak on bare GC electrode. Enantiodiscrimination (here verified, like in the aforementioned ketoprofen case, by testing the drug on either inherently chiral film enantiomer) is very good, reaching a difference of 140 mV evaluated as average of three independent measurements (**Figure 6d**). While the drug is available with L-DOPA only, an experiment with L- and D-DOPA enantiomers in aqueous solution resulting in specular response on R- and S- films is reported in SI.9.

Work is in progress to develop a mechanistic interpretation of such wide-scope enantiorecognition performances in terms of potential differences. Since CV peaks, including chemically and electrochemically reversible ones, appear to undergo rigid shifts rather than morphology changes, the effect should be of thermodynamic rather than kinetic character. In particular, it could involve diastereomeric and therefore energetically different intermolecular interactions between enantiopure selector and enantiopure probe. Such interactions could particularly rely on the available aromatic rings, heteroatoms and oligomer ringlets. A further possible alternative or synergic explanation, based on the internal magnetic field of the chiral film, will be outlined in the next paragraph.

5.3 Interaction with electron spin magnetic moments

Enantiopure electrodeposited oligo-**1** films also gave outstanding performances when tested in magnetoelectro-chemistry experiments as molecular spin filters, of potential interest in spintronics. In particular, CV patterns were recorded for an achiral, reversible Fe(III)/Fe(II) couple in aqueous solution, on ITO electrode modified with a very thin oligo-**1** film, under application of an external magnetic field

(more details are reported in **SI.1.6**). A wide shift in the couple redox potential was observed upon flipping the north/south magnet orientation or changing the (*R*)- or (*S*)- enantiopure film configuration (**Figure 7**), the same striking behaviour very recently observed by some of us[9] working on inherently chiral oligo-**BT$_2$T$_4$** films and even on PEDOT films with stereocenters as stereogenic elements, but characterized by C_2 symmetry, analogously to the atropisomeric inherently chiral oligomers, favouring supramolecular helicoidal assemblies.[39] Such effect has been tentatively justified in terms of "spin-modulated electrochemical potentials" considering the effect of internal and external magnetic field on the electron energy levels as a function of their α or β spin magnetic moment.[9] Recording CV patterns for the achiral redox probe on bare ITO under external magnetic field, or on ITO modified with an inherently chiral film, implying a local "internal" magnetic field, but without applying an external one, results in no potential dif-ference upon changing the N *vs* S magnet orientation in the first case, or the (*R*)- *vs* (*S*)- film configuration in the second ca-se.[9] This is reasonable, since a single magnetic field, be it an applied external one or the internal "chiral" one of an enantio-pure thin layer, should result in energy level splitting for α and β electrons, but specular inverting magnetic field orientation or film configuration; thus the two situations are energetically equivalent, resulting in no difference in the observed redox pe-ak potential. Instead combining the internal and external mag-netic fields yields two different couples of equivalent α,β ener-gy level splitting situations, one corresponding to internal and external magnetic field favouring the same spin orientation and the other one to them having antagonist effects; such situations are reciprocally diastereomeric and therefore ener-getically different, which could justify the CV peak differences.[9] Achieving spin-modulated electrochemical potentials looks a very attractive tool for possible advanced applications, consi-dering the intrinsic convenience of electrode potential for selection, activation, or transduction purposes. Moreover it also suggests an additional interpretative scheme for the po-tential differences observed when applying enantiopure inhe-rently chiral film electrodes to the discrimination of enan-tiopure molecular probes (paragraph **5.2**). In fact, diastereo-meric changes in the α,β electron energy level splittings, with related differences in redox potentials, could not only be induced by the combination of the (*S*)- or (*R*)- internal mag-netic field of the chiral enantiopure film with a NS or SN ex-ternal one, but also by the modulation of the (*S*)- or (*R*)- in-ternal magnetic field by the presence of either a (*S*)- or a (*R*)- chiral probe. We look forward to performing further investi-gations concerning this important feature.

5.4. Analogies and connections among the former all-around chiral discrimination performances

The above described threefold enantiodiscrimination ability of biindole-based film selectors, together with a similar pool of performances of bibenzothiophene-based selectors collectable

from a combination of previous works[1-6], highlights fascinating symmetries and connections between chiral electrochemistry, chiroptics and spintronics (which could be tentatively summarized as in **Scheme SI.11**). The connections (notwithstanding the known differences between electrical and optical energy gap[45]) between electronic absorption spectroscopy, dealing with intramolecular electron transitions, and voltammetry/potentiodynamic electrochemistry, dealing with molecule to electrode/electrode to molecule electron transfers, are now confirmed at an increased complexity level, with the addition of chirality to the two interacting actors, *i.e.* in the first case working with (*S*)- or (*R*)- chiral molecular probes and L- or D-circularly polarized light components in electronic *circular dichroism* spectroscopy; in the second case working with (*S*)- or (*R*)- chiral molecular probes and (*S*)- or (*R*)- inherently chiral electrodes in *enantioselective* voltammetry. To start with, the "ideal selector check-list" resulting in effective chiral voltammetry with wide ΔE potential diffe-ren-ces for the antipodes of molecular electroactive probes[33], strikingly corresponds to the features resulting in "top class" ECD chromophores[21,22,40,41], both of them hinging on inherent chirality, amplified through regioregularity in heli-cal/foldamer macro- or supramolecular structures. Thus our benzothiophene or biindole based selectors result in both very wide ΔE potential differences and sharp $\Delta\varepsilon$ ECD features (as well as, symmetrically to ECD, intense CPL). Furthermore, as already pointed out, our atropisomeric monomers, implying two redox sites (in CV) as well as two chromophores (in spectroscopy) equivalent and partially interacting, display the same loss of degeneracy between redox sites (resulting in a twin peak system with a ΔE splitting in cyclic voltammetry) or chromophore energy levels (resulting in $\Delta\lambda$ splitting, unperceived in normal absorption spectra, but evidenced in dichroism ones), both effects being related to reciprocal interactions depending on the torsional angle.[22] Finally a striking analogy is represented by the response of both techniques to an achiral probe under an external applied mag-netic field. The CV experiments performed on our inherently chiral electrodes under applied magnetic field, resulting in potential differences for achiral redox couples upon flipping the magnetic field orientation, very nicely parallel the long known "magnetic ECD" (MCD) experiments[42-44], in which an ECD response is obtained for achiral chromophores under an external applied magnetic field, with mirror image spectrum upon changing field orientation.
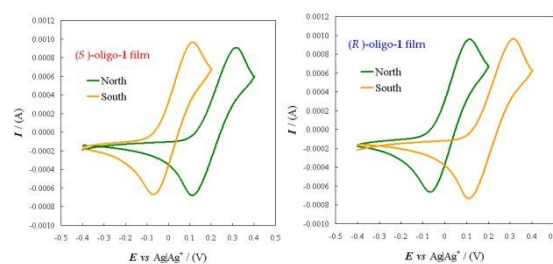

Figure 7. CV patterns for the achiral Fe(CN)$_6^{3-}$|Fe(CN)$_6^{4-}$ redox couple, recorded

at 0.05 V/s in aqueous solution on ITO electrodes modified by a thin layer of (*S*)- or (*R*)- enantiopure oligo-**1** thin film (right and left box, respectively), applying an

external magnet with NS or SN orientation (green or orange lines respectively).

6. Conclusions

The striking performances of biindole-based inherently chiral molecular materials confirm the general validity of the "inherent chirality" strategy. The family provides a new attractive tool with all-around enantiodiscrimination ability, to be possibly exploited for applications in chiral electrochemistry, chiroptics as well as spintronics, three fields which appear to share fascinating fundamental correlations to be further explored.

We particularly look forward to extending the study to other inherently chiral selectors, also including ionic liquid/additive ones, and to ternary combinations (for instance, circular dichroism of the inherently chiral film in the presence of a chiral molecular probe, either chromophore or non-chromophore).

There are no conflicts to declare.

Acknowledgements

References

1. F. Sannicolò, S. Arnaboldi, T. Benincori, V. Bonometti, R. Cirilli, L. Dunsch, W. Kutner, G. Longhi, P. R. Mussini., M. Panigati, M. Pierini, S. Rizzo, *Angew. Chem. Int. Ed.,* 2014, **53**, 2623.

2. F. Sannicolò, P. R. Mussini, T. Benincori, R. Martinazzo, S. Arnaboldi, G. Appoloni, M. Panigati, E. Quartapelle Procopio, V. Marino, R. Cirilli, S. Casolo, W. Kutner, K. Noworyta, A. Pietrzyk-Le, Z. Iskierko, K. Bartold, *Chem. Eur. J.,* 2016, **22**, 10839.

3. G. Longhi, S. Abbate, G. Mazzeo, E. Castiglioni, P. Mussini, T. Benincori, R. Martinazzo, F. Sannicolò, *J. Phys. Chem. C,* 2014, **118**, 16019.

4. F. Sannicolò, P. R. Mussini, T. Benincori, R. Cirilli, S. Abbate, S. Arnaboldi, S. Casolo, E. Castiglioni, G. Longhi, R. Martinazzo, M. Panigati, M. Pappini, E. Quartapelle Procopio, S. Rizzo, *Chem. Eur. J.,* 2014, **20**, 15261.

5. S. Arnaboldi, T. Benincori, R. Cirilli, W. Kutner, M. Magni, P. R. Mussini, K. Noworyta, F. Sannicolò. *Chem. Sci.* 2015, **6**, 1706.

6. S. Arnaboldi, T. Benincori, R. Cirilli, S. Grecchi, L. Santagostini, F. Sannicolò, P. R. Mussini, *Anal. Bioanal. Chem.,* 2016, **408**, 7243.

7. S. Arnaboldi, M. Magni, P. R. Mussini, *Curr. Opin. Electrochem.,* 2018, **8**, 60.

8. S. Arnaboldi, S. Grecchi, M. Magni, P. R. Mussini, *Curr. Opin. Electrochem.,* 2018, **7**, 188.

9. T. Benincori, S. Arnaboldi, M. Magni, S. Grecchi, C. Fontanesi, P. R. Mussini, subm. to *Chem. Sci*, Sept. 2018.

10. K. Ray, S. P. Ananathevel, D. H. Waldeck, R. Naaman, *Science* 1999, **283**, 814.

11. S.G. Ray, S.S. Daube, G. LEitus, Z. VAger, R. Naaman, *Phys. Rev. Lett.* 2006, **96**, 036101.

12. B. Göhler, V. Hamelbeck, T.Z. MArkus, M. Kettner, G.F. Hanne, Z. Vager, R. Naaman, H. Zacharias, *Science* 2011, **331**, 894.

13. P.C. Mondal, C. Fontanesi, D. H. Waldeck, R. Naaman, *Acc. Chem. Res.* 2016, **49**, 2560.

14. E. Quartapelle Procopio, T. Benincori, G. Appoloni, P. R. Mussini, S. Arnaboldi, C. Carbonera, R. Cirilli, A. Cominetti, L. Longo, R. Martinazzo, M. Panigati, R. Po', *New J. Chem.,* 2017, **41**, 10009.

15. S. Kang, I. Cha, J. G. Han, C. Song, *Mater. Express,* 2013, **3**, 119.

16. R. C. Larock, E. K. Yum, *J. Am. Chem. Soc.*, 1991, **113**, 6689.

17. G. Abbiati, A. Arcadi, E. Beccalli, G. Bianchi, F. Marinelli, E. Rossi, *Tetrahedron*, 2006, **62**, 3033.

18. U. Boas, A. Dhanabalan, D. R. Greve, E. W. Meijer, *Synlett.*, 2001, **5**, 634.

19. F. Sannicolò, S. Rizzo, T. Benincori, W. Kutner, K. Noworyta, J. W. Sobczak, V. Bonometti, L. Falciola, P. R. Mussini., M. Pierini. *Electrochim. Acta*, 2010, **55**, 8352.

20. T. Benincori, G. Appoloni, P. R. Mussini, S. Arnaboldi, R. Cirilli, E. Quartapelle Procopio, M. Panigati, S. Abbate, G. Mazzeo, G. Longhi, *Chem. Eur. J.* 2018, **284**, 513.

21. N. Berova, L. Di Bari, G. Pescitelli, *Chem. Soc. Rev.* 2007, **36**, 914.

22. J. T. Vázquez, *Tetrahedron: Asymmetry* 2017, **28**, 1199.

23. J. P. Riehl, G. Muller, in *Comprehensive Chiroptical Spectroscopy*, ed. N. Berova, P. L. Polavarapu, K. Nakanishi, R. W. Woody, Wiley, Hoboken, NJ, 2012, 3, 65.

24. E. Sànchez-Carnerero, A. R. Agarrabeitia, F. Moreno, B. L. Maroto, G. Muller, M. J. Ortiz, S. De la Moya, *Chem. Eur. J.,* 2015, **21**, 13488.

25. G. Longhi, E. Castiglioni, J. Koshoubu, G. Mazzeo, S. Abbate, *Chirality,* 2016, **28**, 696.

26. H. Tanaka, Y. Inoue, T. Mori, *ChemPhotoChem,* 2018, **2**, 1.

27. N. Harada, K. Nakanishi, N. Berova, in *Comprehensive*

Chemical Science Accepted Manuscript

Chemical Science Accepted Manuscript

Chiroptical Spectroscopy, ed. N. Berova, P. L. Polavarapu, K. Nakanishi; R. W. Woody, Wiley, Hoboken, NJ, 2012, 4, 115.

28. U. Narayanan, T. A. Keiderling, *J. Am. Chem. Soc.,* 1983, **105**, 6406.

29. T. Taniguchi, K. Monde, *J. Am. Chem. Soc.*, 2012, **134**, 3695.

30. S. Abbate, G. Mazzeo, S. Meneghini, G. Longhi, S. E. Boiadjiev, D. A. Lightner, *J. Phys. Chem. A*, 2015, **119**, 4261.

31 C. L. Covington, V. P. Nicu, P. L. Polavarapu, *J. Phys. Chem. A*, 2015, **119**, 10589.

32 G. Mazzeo, S. Abbate, G. Longhi, E. Castiglioni, S. E. Boiadjiev, D. A. Lightner, *J. Phys. Chem. B,* 2016, **120**, 2380.

33. E. Castiglioni, S. Abbate, G. Longhi. Appl. Spectrosc. 2010, **64**, 1416.

34. S. Abbate, T. Bruhn, G. Pescitelli, G. Longhi, *J. Phys. Chem. A*, 2017, **121**, 394

35. H. P. J. M. Dekkers in Circular Dichroism: Principles, Applications, ed. N. Berova, K. Nakanishi, R. W. Woody, John Wiley & Sons, NY, 2000, **7**, 185.

36. G. Longhi, E. Castiglioni, S. Abbate, F. Lebon, D. A. Lightner. Chirality, 2013, **25**, 589.

37. S. Abbate, G. Longhi, F. Lebon, E. Castiglioni, S. Superchi, L. Pisani, F. Fontana, F. Torricelli, T. Caronna, C. Villani, R. Sabia, M. Tommasini, A. Lucotti, D. Mendola, A. Mele, D. A. Lightner, J. Phys. Chem. C, 2014, **118**, 1682.

38. G. Longhi, E. Castiglioni, C. Villani, R. Sabia, S. Menichetti, C. Viglianisi, F. Devlin, S. Abbate. *J. Photobiol. Photochem. A: Chemistry*, 2016, **331**, 138.

39. B. M. W. Langeveld-Voss, R. A. J. Janssen and E. W. Meijer, *J. Mol. Struct.* 2000, **521**, 285.

40. G. Pescitelli, L. Di Bari, N. Berova, *Chem. Soc. Rev.* 2011, **40**, 4603.

41. G. Pescitelli, L. Di Bari, N. Berova, *Chem. Soc. Rev.* 2014, **43**, 5211.

42 P.J. Stephens, *Ann. Rev. Phys. Chem.* 1974, **25**, 201.

43 P.J. Stephens, *Adv. Chem. Phys.* 1976, **35**, 197.

44 W.R. Mason, A Practical Guide to Magnetic Circular Dichroism Spectroscopy. Wiley & Sons, Inc. 2007.

45 J.-L. Bredas, *Mater. Horiz.* 2014,**1**,17.

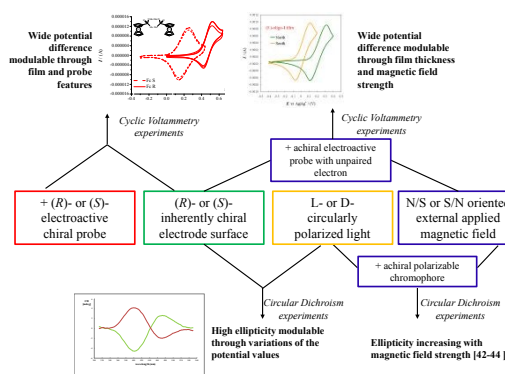# Highly Enantioselective "Inherently Chiral" Electroactive Materials Based on the 2,2'-Biindole Atropisomeric Scaffold

Serena Arnaboldi,[a] Tiziana Benincori,*[b] Andrea Penoni,[b] Luca Vaghi,[c] Roberto Cirilli,[d] Sergio Abbate,[e] Giovanna Longhi,[e] Giuseppe Mazzeo,[e] Sara Grecchi,[a] Monica Panigati[a,f] and Patrizia Romana Mussini*[a]

The new inherently chiral material shows outstanding chirality manifestations with chiral probes, as well as with circularly polarized light components and electron spins.